

Article

Influence of Alkali Metal Ions on the Structural and Spectroscopic Properties of Sm³⁺-Doped Silicate Glasses

Israel R. Montoya Matos 

Department of Civil Engineering, Universidad de Lima, Av. Javier Prado Este 4600, Lima 15023, Peru; imontoya@ulima.edu.pe

Abstract: In the present work, the influence of alkali ions (Li, Na, K) on the structural and spectroscopic properties of silica glasses doped with Sm³⁺ was investigated. Infrared and Raman spectroscopy techniques were used to investigate the structural properties of the alkali silicate glasses. The optical absorption showed bands characteristic of Sm³⁺ ions in alkali silicate glasses, and this was investigated. The Judd–Ofelt theory was applied to evaluate the phenomenological intensity parameters (Ω_2 , Ω_4 , and Ω_6) of the optical absorption measurements. The multi-channel visible and near infrared emission transitions originating from the ⁴G_{5/2}-emitting state of the Sm³⁺ in alkali silicate glasses with a maximum phonon energy of ~1050 cm⁻¹ were investigated. From the evaluated Judd–Ofelt parameters, radiative parameters such as spontaneous emission probabilities, radiative lifetimes, branching ratios, and stimulated emission cross-sections were calculated. The recorded luminescence spectra regions revealed intense green, orange, red, and near-infrared emission bands, providing new traces for developing tunable laser and optoelectronic devices.

Keywords: alkali metal; structural and spectroscopic properties; Judd–Ofelt parameters



Citation: Matos, I.R.M. Influence of Alkali Metal Ions on the Structural and Spectroscopic Properties of Sm³⁺-Doped Silicate Glasses. *Ceramics* **2023**, *6*, 1788–1798. <https://doi.org/10.3390/ceramics6030109>

Academic Editors: Gilbert Fantozzi, Georgiy Shakhgildyan and Michael I. Ojovan

Received: 11 July 2023

Revised: 4 August 2023

Accepted: 17 August 2023

Published: 21 August 2023



Copyright: © 2023 by the author. Licensee MDPI, Basel, Switzerland. This article is an open access article distributed under the terms and conditions of the Creative Commons Attribution (CC BY) license (<https://creativecommons.org/licenses/by/4.0/>).

1. Introduction

Due to their potential for use as lasers and phosphors in a variety of hosts, including glasses, crystals, and transparent vitro-ceramics that exhibit luminescent transitions in the VIS and NIR spectra regions, Ln³⁺-doped ions have attracted considerable technological interest [1]. According to research, the optical spectra of the rare earth ions can be used as structural probes to determine the local field parameters within a specific host glass because the energy levels, profiles, and intensities of the absorption and emission bands depend on how charges are distributed in the first coordination shells of the rare earth ions [2,3]. In oxide glasses, silicate glasses are one of the most popular glass hosts for making optical fiber lasers and amplifiers. Several papers have been published on the optical properties of rare earth ions in different glasses [4–6], but only a few of them have been concerned with Sm³⁺ [7–10]. The significant energy gap (less non-radiative decay) between the ⁴G_{5/2} level and the next lower-lying energy level, ⁶F_{11/2}, which is roughly 7200 cm⁻¹, causes glasses doped with Sm³⁺ ions to have relatively high quantum efficiencies. It has been known for a long time that Sm³⁺ ion provide very strong luminescence in the orange and red spectral regions in a variety of lattices [11,12]. However, only a few attempts have been made to explore the possibility of using the orange-red luminescence of Sm³⁺ ions for the development of visible optical devices. The main reason for not carrying out spectral studies on Sm³⁺ ions doped in glasses is the complicated structure of the 4f⁶ configuration of this ion because these glasses show different channels that lead to luminescence-quenching and have strong phosphorescent intensities [13].

In the present work, the spectroscopic properties of Sm³⁺ ions were used to investigate the local structures of alkali (i.e., Li, Na, and K) oxides in silica. It has been known for a long time that the gradual replacement of one alkali oxide by another induces nonlinear changes in certain physical properties of glasses [14,15], and the explanation for this effect in terms of the atomic structure is not simply due to the amorphous nature of the glass.

2. Materials and Methods

Silicate glasses have the following composition: $33.0 \text{ R}_2\text{O} + 66.0 \text{ SiO}_2 + 1.0 \text{ Sm}_2\text{O}_3$ (mol%), where R = Li, Na, and K. The glasses were prepared using the traditional melting quenching technique. The laboratory chemicals used included purified sand Li_2CO_3 , Na_2CO_3 , K_2CO_3 , SiO_2 , and Sm_2O_3 (99.99% purity grade from Sigma-Aldrich (St. Louis, MO, USA)), and these were used for sample preparation. Since carbonates and silica are highly hygroscopic, they were dried at $200 \text{ }^\circ\text{C}$ for 1–2 h. The mixture was placed in a platinum crucible and heated at 700 to $800 \text{ }^\circ\text{C}$ to eliminate CO_2 [16], and then it was melted at $1550 \text{ }^\circ\text{C}$ for 2 h in air. The melted mixture was quickly poured into a preheated stainless steel mold and annealed at $350 \text{ }^\circ\text{C}$ for 4 h. After that, it was cooled down slowly to room temperature at a rate of $5 \text{ }^\circ\text{C}/\text{min}$. Table 1 shows the compositions, appearances, and melting temperatures of the prepared samples.

Table 1. Chemical compositions of the glass samples.

Sample Notation	Glass Compositions (mol%)	Glass Appearances	Melting Temperatures ($^\circ\text{C}$)
LS-Sm	$33.0 \text{ Li}_2\text{O} + 66.0 \text{ SiO}_2 + 1.0 \text{ Sm}_2\text{O}_3$	Transparent glass	1550
NS-Sm	$33.0 \text{ Na}_2\text{O} + 66.0 \text{ SiO}_2 + 1.0 \text{ Sm}_2\text{O}_3$	Transparent glass	1550
KS-Sm	$33.0 \text{ K}_2\text{O} + 66.0 \text{ SiO}_2 + 1.0 \text{ Sm}_2\text{O}_3$	Transparent glass	1550

The densities of the prepared samples were measured using the Archimedes method (with an analytical balance Shimadzu AUW220D, 0.1 mg/0.01 mg) using distilled water as the immersion liquid. The refractive index was measured using a SOPRA GES-5E ellipsometer. The FTIR transmittance spectra were measured using a Bomem MB100 spectrometer using KBr pellets. The Raman spectra were measured using an HeNe laser as the excitation source. The absorption spectra in the UV-Vis-Nir region were recorded using a high-performance spectrometer (PerkinElmer model LAMBDA 1050) with a spectral resolution of 0.2 nm. The photoluminescence (PL) data were measured using a CryLas GmbH 488 nm CW laser as a pumping source. The PL signal was dispersed by an Acton SP 2300 monochromator and detected by a Pixis 256E CCD. The detected signal was fed to an SR 430 multichannel analyzer and transferred to a computer running acquisition software (OriginPro).

3. Results and Discussions

3.1. Structural Analysis

One of the most successful techniques for structural analysis is infrared spectroscopy, which makes it possible to identify structural features related to both the anionic sites containing the modifying cations and the local units that form the glass network [17]. Figure 1 shows the vibrational spectra of the alkali silicate glasses, which exhibit prominent bands at $\sim 1037 \text{ cm}^{-1}$ for LS, $\sim 1060 \text{ cm}^{-1}$ for NS, and $\sim 1013 \text{ cm}^{-1}$ for KS due to Si–O–Si stretching within the tetrahedral by the presence of alkali ions. These bands are sharpened by the addition of rare earth ions. The introduction of rare earth ions in the matrix will alter the environment of the defect centers in the silica [18]. Also, the relative intensities of the peaks corresponding to the Si–O stretching from the tetrahedral and the non-bridged Si–O were nearly the same for the LS and NS samples, but for the KS sample, it was possible to observe a shift in the band at $\sim 1013 \text{ cm}^{-1}$ to lower wavenumbers, suggesting that the effect of K on the Si–O stretching within the tetrahedral was slightly different from that of Li and Na. The bands at $\sim 916 \text{ cm}^{-1}$ for LS, $\sim 891 \text{ cm}^{-1}$ for NS, and 884 cm^{-1} for KS were due to the stretching of the non-bridged terminal Si–O. The addition of alkali ions would decrease the local symmetry due to the formation of non-bridging oxygen bonds, giving rise to a stretching mode at $\sim 900 \text{ cm}^{-1}$ [19]. Comparing the spectra shown in Figure 1 and described in Table 2, all of them presented shoulders at $\sim 900 \text{ cm}^{-1}$, though they were more pronounced for LS and NS samples, indicating the formation of non-bridged terminal Si–O.

The bands at $\sim 774\text{ cm}^{-1}$ for LS, $\sim 752\text{ cm}^{-1}$ for NS, and $\sim 745\text{ cm}^{-1}$ for KS were due to the stretching of the bridged Si–O–Si symmetric vibrations; more precisely, they were due to the bending mode of the bridging oxygen perpendicular to the Si–Si axis within the Si–O–Si plane and were at $\sim 470\text{ cm}^{-1}$ for LS and NS and $\sim 450\text{ cm}^{-1}$ for KS due to the Si–O rocking motion.

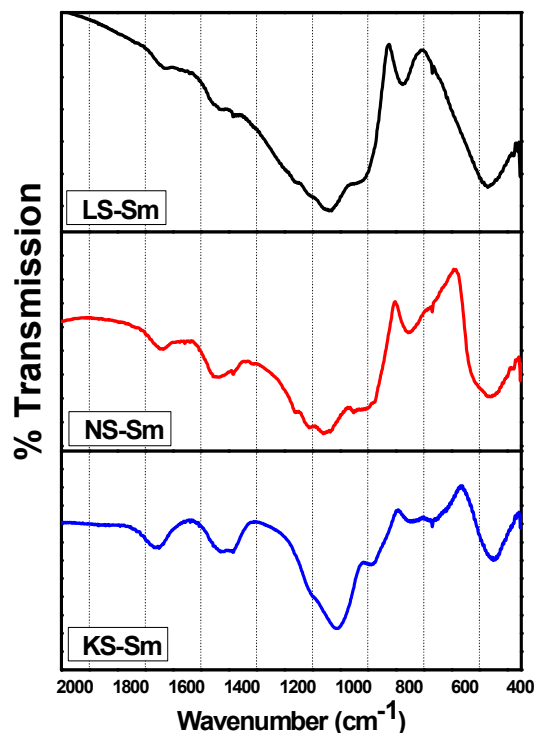


Figure 1. FTIR absorption spectra of the different alkali silicate glasses.

Table 2. Vibration mode FTIR spectra of the alkali silicate glasses.

Vibration Mode	LS-Sm	NS-Sm	KS-Sm
	Wavenumber (cm^{-1})	Wavenumber (cm^{-1})	Wavenumber (cm^{-1})
Si–O–Si bending vibration	472	468	447
O–Si–O bending vibration	774	752	745
Si–O–Si symmetric stretching	916	891	884
Si–O–Si asymmetric stretching	1037	1060	1013

Figure 2 shows the Raman spectra of the samples. These spectra consisted of three intense peaks as representative cases, and the band assignments are presented in Table 3. Prominent features of the silica glass Raman spectrum were shown in Matson et al. [20]. The Raman spectrum of silica contains a large and asymmetric band near $\sim 440\text{ cm}^{-1}$ and a sharp band at $\sim 492\text{ cm}^{-1}$ related to the SiO_4 tetrahedra. A broad band at $\sim 800\text{ cm}^{-1}$ is related to the network of the SiO_2 glass, a band at $\sim 600\text{ cm}^{-1}$ is related to defects, bands at 1060 and 1190 cm^{-1} are related to Si–O–Si vibrations, and a band at $\sim 950\text{ cm}^{-1}$ is related to crystalline metasilicates containing chains of SiO_4 tetrahedra. According to Matson et al. [20], the introduction of alkali ions in the silica network induces changes in the Raman spectrum depending on the ion type and concentration. The stretching of non-bonding oxygen on SiO_4 tetrahedra due to the alkali ion appeared at $\sim 1100\text{ cm}^{-1}$ [20]. The results shown in Figure 2 showed that intense bands were observed for all samples at close to 600 cm^{-1} , and they were related to defects in the silica network and were likely induced by the alkali ions (the creation of non-bonding oxygen atoms). Consistently, the bands close to $\sim 1100\text{ cm}^{-1}$ and $\sim 950\text{ cm}^{-1}$ were also observed for all samples while the band at $\sim 800\text{ cm}^{-1}$,

related to the silica network, was not observed. This suggested that the incorporation of the rare earth oxides studied in the alkali silicate glasses caused more non-bridging oxygen to occur, and consequentially, it led to more polymerization in the network. It is expected that the presence of rare earth oxides as modifiers contribute three NBO (non-bridging-oxygen) atoms to a glass system while traditional modifiers (Li_2O , Na_2O , and K_2O) contribute only one NBO (non-bridging-oxygen) atom [21].

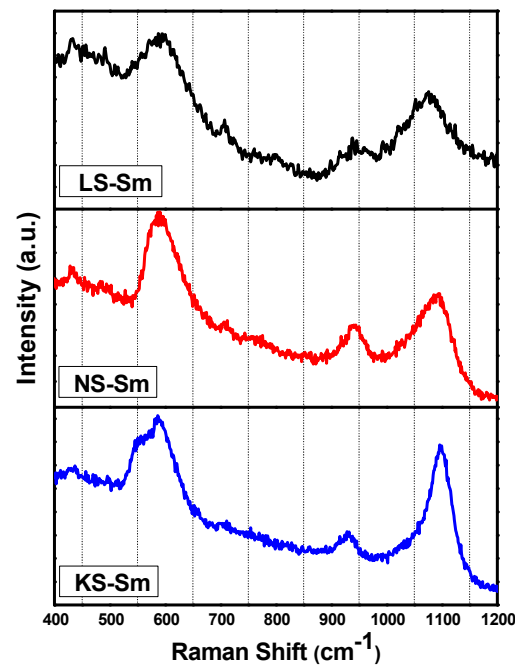


Figure 2. Raman spectra of the different alkali silicate glasses.

Table 3. Vibration-mode Raman spectra of the alkali silicate glasses.

Vibration mode	LS-Sm	NS-Sm	KS-Sm
	Wavenumber (cm^{-1})	Wavenumber (cm^{-1})	Wavenumber (cm^{-1})
Si–O	591	589	587
Si–O–Si symmetric stretching	939	942	930
Si–O–Si antisymmetric stretching	1073	1094	1097

Physical parameters such as the densities, refractive indexes, concentrations of Sm^{3+} ions, polaron radii, inter-ionic distances, field strengths, reflection losses, optical dielectrics, and dielectric constants of the glasses were calculated using standard equations [22,23] and are presented in Table 4.

3.2. Optical Properties

The absorption bands of the RE ions in a host glass can be expressed as oscillator strengths, and the electronic transitions can be calculated using the expression:

$$f_{\text{exp}} = 4.318 \times 10^{-9} \int \varepsilon(\nu) d\nu \quad (1)$$

where the integral represents the area under the absorption curve and $\varepsilon(\nu)$ is the molar extinction coefficient. According to the Judd–Ofelt (JO) theory [24,25], which defines a set of three parameters (Ω_2 , Ω_4 , and Ω_6) susceptible to the environment of the RE ion, the parameter Ω_2 is related to the covalence of the metal–ligand bond while Ω_4 and Ω_6 are related to the rigidity of the host matrix. In the Judd–Ofelt theory, the oscillator strength,

f_{cal} , of the spectral intensity of an electric dipole absorption transition from the initial state, aJ , to the final state, bJ' ,

$$f_{cal}(aJ, bJ') = \frac{8\pi^2 m c v}{3h(2J+1)} \left[\frac{(n^2+2)^2}{9n} \right] x \sum_{\lambda=2,4,6} \Omega_{\lambda} \langle aJ | U^{\lambda} | bJ' \rangle^2 \quad (2)$$

where m is the mass of an electron, c is the velocity of the light, h is the Planck's constant, v is the wavenumber of the absorption peak, n is the refractive index, and U^{λ} is the doubly reduced matrix element.

Table 4. Physical properties of the Sm³⁺-doped alkali metal ion silicate samples.

Physical Properties	LS-Sm	NS-Sm	KS-Sm
Density, ρ (gm/cm ³) (± 0.0005)	2.4552	2.5396	2.5598
Refractive index (n) (585 nm)	1.4930	1.4490	1.4310
Concentration of Sm ³⁺ , N ($\times 10^{20}$ ions/cm ³)	2.1896	1.8854	1.7370
Molar volume (V_m) (cm ³ /mol)	27.5024	31.9404	34.6697
Polaron radius, r_p (Å)	6.6846	7.0264	7.2211
Interionic distance, r_i (nm)	1.6591	1.7439	1.7923
Field strength, F ($\times 10^{16}$ cm ⁻²)	6.7139	6.0766	5.7533
Reflection losses (R_L) ($\times 10^{-2}$)	3.9107	3.3614	3.1433
Molar refraction (R_m) (cm ³ /mol)	7.9928	8.5671	8.9742
Optical dielectric constant ($P\partial t/\partial P$)	1.2290	1.0996	1.0478
Dielectric constant (ϵ)	2.2290	2.0996	2.0478
Molar polarizability (α_m) $\times 10^{-22}$ cm ³	3.1687	3.3964	3.5578

The optical absorption spectra of the Sm³⁺-doped different alkali silicate glasses (Li, Na, and K) recorded at temperature room are shown in Figure 3. The spectral behavior of the Sm³⁺ in the glasses was very similar to that found in fluorophosphate [26], borosulphate [27], and germanate [28] glasses. Seven absorption bands were shown for each sample, as described in Table 5, which were associated with the absorption transitions from the ⁶H_{5/2} ground state to the excited states, as labeled in Figure 3. The observed band positions of different absorption peaks of the samples were due to the interactions between the alkali ions and the crystal field. The band shapes of the ions in all three alkali silicate glasses were similar, with small differences in the half-band widths and peak positions. These results suggested that the Sm³⁺ ions resided in essentially the same sites as the three alkali ions. The calculated $\bar{\beta}$ and δ values of the glasses are presented in Table 5. The observed the nephelauxetic effect [29,30] was increased with the increase in the alkali ions as follows: K > Na > Li. The negative results demonstrated that the Sm³⁺ ions and their surrounding ligands were primarily ionic in character. Sm³⁺ has a 4f⁵ electron configuration which is characterized by ²⁵⁺¹L_J free-ion levels. With knowledge of the Sm³⁺ concentrations, sample thicknesses, peaks positions, and peak areas, the experimental oscillator strengths were obtained by using Equation (1). From the experimentally measured oscillator strengths and doubly reduced matrix elements [31], the J–O intensity parameters were obtained using Equation (2). The measured, as well calculated, oscillator strengths and J–O intensity parameters of the Sm³⁺ in the alkali silicate glasses are presented in Tables 6 and 7, respectively. The magnitudes of J–O intensity parameters are important for investigations of glass structures and transition properties of rare earth ions. In general, the Ω_2 parameter is an indicator of the covalence of a metal–ligand bond (short-range effect) and the Ω_4 and Ω_6 parameters provide information about the rigidity of a host glass's matrix (long-range effects) [32].

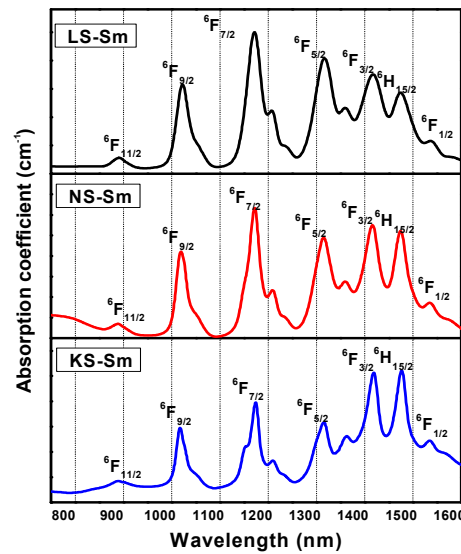


Figure 3. Optical absorption spectra of the Sm³⁺-doped alkali silicate glasses recorded at room temperature in the NIR region.

Table 5. Bands positions (cm⁻¹) and their assignments for the Sm³⁺-doped alkali silicates.

Transitions ⁶ H _{5/2}	LS-Sm	NS-Sm	KS-Sm
⁶ F _{11/2}	10,626.99	10,655.73	10,672.36
⁶ F _{9/2}	9325.81	9353.91	9369.21
⁶ F _{7/2}	8185.95	8183.33	8169.19
⁶ F _{5/2}	7316.94	7325.95	7322.03
⁶ F _{3/2}	6815.18	6821.16	6806.60
⁶ H _{15/2}	6558.67	6560.53	6549.88
⁶ F _{1/2}	6288.49	6306.04	6309.73
β	1.01436	1.01569	1.01573
δ	-0.01416	-0.01544	-0.01548

Table 6. Experimental (*f_{exp}*) and calculated (*f_{cal}*) oscillator strengths ($\times 10^{-6}$) and rms (σ_{rms}) for the Sm³⁺ alkali silicate glasses.

Transitions ⁶ H _{5/2}	LS-Sm		NS-Sm		KS-Sm	
	<i>f_{exp}</i>	<i>f_{cal}</i>	<i>f_{exp}</i>	<i>f_{cal}</i>	<i>f_{exp}</i>	<i>f_{cal}</i>
⁶ F _{11/2}	0.602	0.568	0.363	0.407	0.309	0.205
⁶ F _{9/2}	4.720	3.440	3.390	2.470	1.640	1.230
⁶ F _{7/2}	3.490	4.660	2.490	3.33	1.220	1.610
⁶ F _{5/2}	2.360	1.890	1.630	1.370	0.648	0.595
⁶ F _{3/2}	1.210	1.060	1.170	0.874	0.760	0.475
⁶ H _{15/2} + ⁶ F _{1/2}	0.897	0.326	1.091	0.383	0.806	0.307
σ_{rms}	0.9856		0.8310		0.5036	

In the values for Ω_2 , Ω_4 , and Ω_6 in Table 7 for the Sm³⁺-doped alkali silicate glasses, we observed variations in the intensities of the parameters as follows: $\Omega_6 > \Omega_4 > \Omega_2$. The lithium silicate glass matrix exhibited higher Ω_2 values and the potassium silicate glass matrix was minimal, indicating lower covalence values for these compositions. It has been proposed that in oxide glasses, a rare earth ion is surrounded by eight neighboring oxygen atoms belonging to the corners of SiO₄, forming a tetrahedral. Normally, the intensity parameter Ω_2 , which indicates covalence, decreases with decreases in the intensity of the hypersensitive transition.

The hypersensitive transitions for the Sm³⁺ ions were ⁶H_{5/2}→⁶F_{1/2} and ⁶F_{3/2}. The hypersensitivity of a transition is proportional to the nephelauxetic ratio, indicating the RE–O bond’s ionic nature [33]. The Ω₆ parameter was the largest in the glasses, showing that the Sm–O bond was more ionic in these glasses than in other glasses and indicating the higher rigidity of the glasses. The shift in the peak wavelengths of the hypersensitive transitions towards shorter wavelengths increased with the size of the alkali ions in the glass matrix, indicating decreases in the ionic nature of the RE–O bonds. Also, these changes were not the result of a large-scale structural rearrangement of the local glass network, but rather, they were primarily caused by the interactions between the alkali ions and the matrix.

Table 7. A comparison of the Judd–Ofelt parameters (Ω_λ) (×10^{−20} cm²) in different hosts.

Host Matrix	Ω ₂	Ω ₄	Ω ₆	χ = Ω ₄ /Ω ₆	Order
LS-Sm ³⁺ (present work)	1.28	3.14	4.53	0.69	Ω ₆ > Ω ₄ > Ω ₂
LCN borate [34]	0.84	4.00	5.02	0.79	Ω ₆ > Ω ₄ > Ω ₂
30Li ₂ O:70B ₂ O ₃ -Pr ³⁺ [35]	0.10	4.71	5.28	0.89	Ω ₆ > Ω ₄ > Ω ₂
NS-Sm ³⁺ (present work)	1.27	2.69	3.15	0.85	Ω ₆ > Ω ₄ > Ω ₂
NaZnBS-Sm ³⁺ [27]	0.55	9.68	9.77	0.99	Ω ₆ > Ω ₄ > Ω ₂
30Na ₂ O:70B ₂ O ₃ -Pr ³⁺ [35]	0.98	4.76	4.86	0.97	Ω ₆ > Ω ₄ > Ω ₂
KS-Sm ³⁺ (present work)	1.04	1.12	1.61	0.69	Ω ₆ > Ω ₄ > Ω ₂
KZnBS-Sm ³⁺ [27]	0.18	11.37	11.45	0.99	Ω ₆ > Ω ₄ > Ω ₂
LKG [11]	0.63	4.05	4.69	0.86	Ω ₆ > Ω ₄ > Ω ₂

3.3. Emission Spectra and Radiative Properties

The emission spectra under the 488 nm excitation wavelength consisted of potential green, yellow, and orange-reddish emissions at ~565 nm (⁴G_{5/2}→⁶H_{5/2} magnetic dipole (MD) transition), ~600 nm (⁴G_{5/2}→⁶H_{7/2} mixed magnetic-electric dipole transition), ~650 nm (⁴G_{5/2}→⁶H_{9/2} electric dipole transition), and ~710 nm (⁴G_{5/2}→⁶H_{11/2} electronic dipole transition), all of which were recorded at room temperature in the VIS regions, as shown in Figure 4. The peaks in the NIR region centered at ~915 nm (⁴G_{5/2}→⁶F_{3/2}), ~960 nm (⁴G_{5/2}→⁶F_{5/2}), ~1045 nm (⁴G_{5/2}→⁶F_{7/2}), ~1200 nm (⁴G_{5/2}→⁶F_{9/2}), and ~1300 nm (⁴G_{5/2}→⁶F_{11/2}) are presented in Figure 5. It is important to note the largest number of transitions observed, including the one at 1300 nm, indicated that the alkali silicate glasses were very efficient systems.

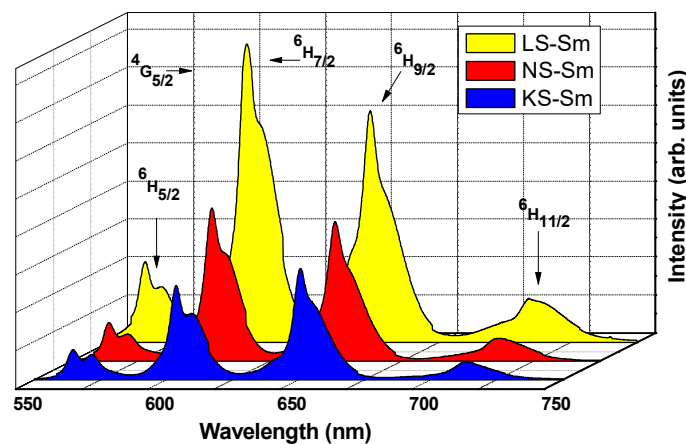


Figure 4. VIS region emission spectra for the alkali silicate glasses under excitation at 488 nm.

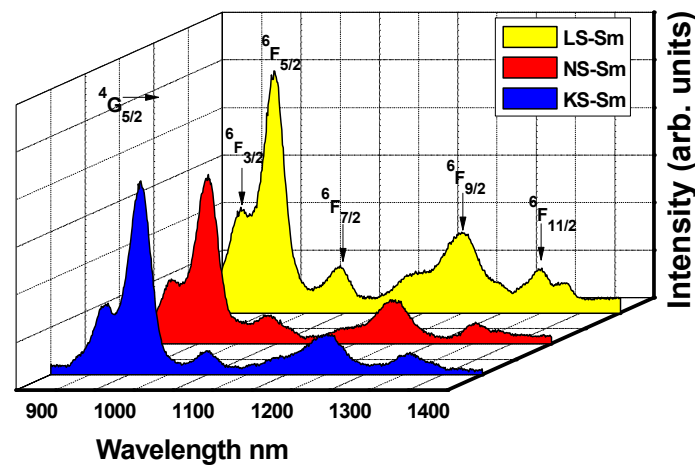


Figure 5. NIR region emission spectra for the alkali silicate glasses under excitation at 488 nm.

The radiative transition probability $A_{rad}(aJ \text{ and } bJ')$ is given by the expression:

$$A_{rad}(aJ, bJ') = \frac{64\pi^4 v^3 e^2}{3h(2J+1)} \left[\frac{n(n^2+2)^2}{9} S_{ed} \right] \tag{3}$$

where S_{ed} and S_{md} are electric and magnetic dipole line-strengths, respectively. From these values, it is possible to calculate the branching ratio and radiative lifetime of an emitting state, aJ , which is calculated from:

$$\beta_{rad}(aJ, bJ') = \frac{A_{rad}(aJ, bJ')}{\sum_{bJ'} A_{rad}(aJ, bJ')} \tag{4}$$

and

$$\frac{1}{\tau_{rad}} = \sum_{bJ'} A_{rad}(aJ, bJ') \tag{5}$$

In addition, another important radiative parameter property, the fluorescent integrated emission cross-section (σ_p) for stimulated emissions, is estimated from the following equation:

$$\sigma_p(aJ, bJ') = \frac{\lambda_p^4}{8\pi c n^2 \Delta\lambda_{eff}} A_{rad}(aJ, bJ') \tag{6}$$

Due to the characteristic lack of long-range order in glasses, the local environment of RE ions is expected to be slightly different from one site to another, resulting in broad absorption bands. The crystal field splitting is also responsible for the broadening of these bands [26]. It has been assumed that in oxide glasses, an RE ion has eight neighboring oxygen atoms that are shared with the corners of the glass, forming a tetrahedral. In lanthanides, there are certain f–f transitions that are exceptionally sensitive to the local environment, and they are known as hypersensitive transitions ($\Delta J \leq 2$, $\Delta L \leq 2$, and $\Delta S = 0$). For Sm^{+3} , they corresponded to the ${}^6H_{5/2} \rightarrow {}^6F_{3/2}$ and ${}^6F_{1/2}$ transitions, which were in the visible range. The addition of alkali ions as network modifiers in oxide glasses induced the formation of non-bridging oxygen atoms, changing the forming cation coordination number. This effect induced changes in the lanthanide–oxygen distances and, therefore, should affect the optical properties of the RE ion in the oxide glass [26].

Using the phenomenological intensity parameters, one can estimate the radiative transition probability values for $A_{rad}(s^{-1})$ (Equation (3)). From these values, it is possible to calculate the branching ratio β_R (Equation (4)) and radiative lifetime τ_{rad} (ms) (Equation (5)) from the ${}^4G_{5/2}$ excited level to all its lower-lying levels for alkali silicate glasses, as shown in Table 8. The stimulated emission cross-section (Equation (6)) is an important parameter for predicting a better laser performance and high quantum efficiency of glass matrices. Table 9

reports the emission band positions, the effective bandwidths, and the values of emission cross-section $\sigma(\lambda_p)$ for some of the transitions originating from the $^4G_{5/2}$ level of the Sm^{3+} ions in the silicate glasses. Even though the magnitudes of the intensity parameters obtained in the present work were low, the measured $\sigma(\lambda_p)$ values for the $^4G_{5/2} \rightarrow ^6H_{7/2, 9/2}$ transitions were relatively higher than those reported for other glasses [36–39]. The highest values were observed for the $^4G_{5/2} \rightarrow ^6H_{7/2}$ transitions ($6.14 \times 10^{-22} \text{ cm}^2$, $4.97 \times 10^{-22} \text{ cm}^2$, and $2.31 \times 10^{-22} \text{ cm}^2$ for the LS, NS, and KS samples, respectively). Despite the values of $\sigma(\lambda_p)$ for the NIR emissions being lower than those of the VIS emissions, they were of the same order of magnitude. Therefore, the novel NIR emissions of the alkali silicate glasses provided a new clue for developing potential NIR optoelectronic devices.

Table 8. Radiative transition probability values ($A_{rad} \text{ (s}^{-1}\text{)}$), branching ratio values (β_R), and radiative lifetime values ($\tau_{rad} \text{ (ms)}$) for the Sm^{3+} -doped alkali silicate glasses.

Transitions from $^4G_{5/2}$ to	LS-Sm				NS-Sm				KS-Sm			
	$\Delta E(\text{cm}^{-1})$	$A_{rad}(\text{s}^{-1})$	β_R	τ_{rad}	$\Delta E(\text{cm}^{-1})$	$A_{rad}(\text{s}^{-1})$	β_R	τ_{rad}	$\Delta E(\text{cm}^{-1})$	$A_{rad}(\text{s}^{-1})$	β_R	τ_{rad}
$^6H_{5/2}$	17,740	45.40	0.1812	3.99	17,731	36.28	0.1951	5.37	17,728	17.19	0.1906	11.08
$^6H_{7/2}$	16,608	110.618	0.4415		16,584	76.318	0.4104		16,568	34.372	0.3808	
$^6H_{9/2}$	15,407	58.314	0.2327		15,408	46.000	0.2473		15,369	25.510	0.2827	
$^6H_{11/2}$	14,101	26.256	0.1048		14,065	18.945	0.1019		14,025	8.074	0.0895	
$^6F_{3/2}$	10,890	0.800	0.0032		10,905	0.705	0.0038		10,834	0.502	0.0056	
$^6F_{5/2}$	10,424	5.925	0.0236		10,395	5.257	0.0283		10,373	3.405	0.0377	
$^6F_{7/2}$	9578	1.965	0.0078		9606	1.505	0.0081		9533	0.606	0.0067	
$^6F_{9/2}$	8324	0.860	0.0034		8326	0.701	0.0038		8321	0.458	0.0051	
$^6F_{11/2}$	7686	0.419	0.0017		7669	0.271	0.0015		7645	0.129	0.0014	

Table 9. Stimulated emission cross-sections ($\sigma(\lambda_p) \times 10^{-22} \text{ cm}^2$) for the emission peak wavelengths (λ_p) in the infrared with the effective line width values (λ_{eff}) for the Sm^{3+} -doped alkali silicate glasses.

Transitions from $^4G_{5/2}$ to	LS-Sm			NS-Sm			KS-Sm		
	$\lambda_p \text{ (nm)}$	$\Delta\lambda_{eff} \text{ (nm)}$	$\sigma(\lambda_p)$	$\lambda_p \text{ (nm)}$	$\Delta\lambda_{eff} \text{ (nm)}$	$\sigma(\lambda_p)$	$\lambda_p \text{ (nm)}$	$\Delta\lambda_{eff} \text{ (nm)}$	$\sigma(\lambda_p)$
$^6H_{5/2}$	564	10.14	2.69	564	11.01	2.11	565	12.28	0.92
$^6H_{7/2}$	602	14.16	6.14	603	12.82	4.97	604	12.68	2.31
$^6H_{9/2}$	649	14.76	4.17	650	14.83	3.49	651	13.73	2.16
$^6H_{11/2}$	710	22.91	1.73	711	21.63	1.42	713	18.75	0.72
$^6F_{3/2}$	919	19.03	0.18	919	17.74	0.18	921	19.60	0.12
$^6F_{5/2}$	959	27.37	1.09	962	28.36	1.01	964	22.92	0.83
$^6F_{7/2}$	1044	27.25	0.51	1043	32.19	0.35	1052	24.68	0.19
$^6F_{9/2}$	1199	70.61	0.15	1201	60.99	0.15	1204	61.82	0.10
$^6F_{11/2}$	1301	39.59	0.18	1309	33.35	0.15	1307	41.09	0.06

4. Conclusions

The present work detailed the influence of alkali ions on the structural and spectroscopic properties of Sm^{3+} ion-doped silicon glasses. The FTIR spectra of the doped silica showed that the Si–O–Si bending modes were sharpened with the introduction of rare earth ions. The addition of alkali ions decreased the local symmetry due to the formation of non-bridging oxygen bonds, giving rise to a stretching mode at $\sim 900 \text{ cm}^{-1}$. The optical properties of the Sm^{3+} alkali silicates were measured and analyzed using the Judd–Ofelt theory. The Ω_6 parameter was the largest in the glasses, showing that the Sm–O bonds were more ionic in these glasses than in other glasses and indicating the higher rigidity of these glasses. The intensities of the emission bands in the VIS and NIR regions of the samples containing Li were relatively high compared to those of the samples containing Na and K. The emission spectra showed potential for green, yellow, and orange-reddish

emissions. The branching ratios were larger for the ${}^4G_{5/2} \rightarrow {}^6H_{7/2}$ (VIS region) transition and decreased from the Li and Na to the K silicates, and the ratios for the ${}^4G_{5/2} \rightarrow {}^6F_{5/2}$ (NIR region) transition decreased as follows: Li > Na > K. The stimulated emission cross-sections obtained were similar to the values reported in the literature for Sm^{3+} in different glasses.

Funding: The author is grateful for the financial support of the Brazilian agencies CAPES, CNPq, and FAPERGS.

Institutional Review Board Statement: Not applicable.

Informed Consent Statement: Not applicable.

Data Availability Statement: Not applicable.

Conflicts of Interest: The author declares no conflict of interest.

References

1. Goodwin, D.W. Spectra and Energy Levels of Rare Earth Ions in Crystals. *Phys. Bull.* **1969**, *20*, 525. [[CrossRef](#)]
2. Gatterer, K.; Pucker, G.; Jantscher, W.; Fritzer, H.P.; Arafa, A. Suitability of Nd (III) absorption spectroscopic to probe the structure of glasses from the ternary system $Na_2O-B_2O_3-SiO_2$. *J. Non-Cryst. Solids* **1998**, *231*, 189–199. [[CrossRef](#)]
3. Sailaja, B.; Joyce Stella, R.; Thitumala Rao, G.; Jaya Raja, B.; Pushpa Manjari, V.; Ravikumar, R.V.S.N. Physical, structural and spectroscopic investigations of Sm^{3+} doped ZnO mixed alkali borate glass. *J. Mol. Struct.* **2015**, *1096*, 129–235. [[CrossRef](#)]
4. Cases, R.; Chamarro, M.A. Judd-Ofelt analysis and multiphonon relaxations of rare earth ions in fluorohafnate glasses. *J. Solid State Chem.* **1991**, *90*, 313. [[CrossRef](#)]
5. Basiev, T.; Dergachev, A.Y.; Orlovskii, Y.V.; Prokhorov, A.M. Multiphonon nonradiative relaxation from high-lying levels of Nd^{3+} ions in fluoride and oxide laser materials. *J. Lumin.* **1992**, *53*, 19. [[CrossRef](#)]
6. Broer, M.M.; Bruce, A.J.; Grodkiewicz, W.H. Resonantly induced refractive index changes in Eu^{3+} - and Er^{3+} -doped silicate and phosphate glasses. *J. Lumin.* **1992**, *53*, 15. [[CrossRef](#)]
7. Reisfeld, R.; Bornstein, A.; Boehm, L. Optical characteristics and intensity parameters of Sm^{3+} in GeO_2 , ternary germanate, and borate glasses. *J. Solid State Chem.* **1975**, *14*, 14. [[CrossRef](#)]
8. Rodriguez, V.D.; Martin, I.R.; Alcalá, R.; Cases, R. Optical properties and cross relaxation among Sm^{3+} ions in fluorozincate glasses. *J. Lumin.* **1992**, *54*, 231. [[CrossRef](#)]
9. Ratnakaram, Y.C.; Thirupathi Naidu, D.; Vijaya Kumar, A.; Gopal, N.O. Influence of mixed alkalis on absorption and emission properties of Sm^{3+} ions in borate glasses. *Phys. B* **2005**, *358*, 296–307. [[CrossRef](#)]
10. Annapurna, K.; Dwivedi, R.N.; Kumar, A.; Chaudhuri, A.K.; Buddhudu, S. Temperature dependent luminescence characteristic of Sm^{3+} -doped silicate glass. *Spectrochim. Acta A Mol. Biomol. Spectrosc.* **2000**, *56*, 103–109. [[CrossRef](#)]
11. Jayasimhadri, M.; Chon, E.-J.; Jang, K.-W.; Lee, H.S.; Kim, S. Spectroscopic properties and Judd-Ofelt analysis of Sm^{3+} doped lead-germanate-tellurite glasses. *J. Phys. D Appl. Phys.* **2008**, *41*, 175101. [[CrossRef](#)]
12. Sharma, Y.K.; Surana, S.S.L.; Singh, R.K. Spectroscopic investigation and luminescence spectra of soda lime silicate glasses. *J. Rare Earths* **2009**, *27*, 773. [[CrossRef](#)]
13. Basavapoornima, C.; Jayasankar, C.K. Spectroscopic and photoluminescence properties of Sm^{3+} ions in Pb-K-Al-Na phosphate glasses for efficient visible lasers. *J. Lumin.* **2014**, *153*, 233–241. [[CrossRef](#)]
14. Isard, J.O. The mixed alkali effect in glass. *J. Non-Cryst. Solids* **1969**, *1*, 235–261. [[CrossRef](#)]
15. Day, D.E. Mixed alkali glasses—Their properties and uses. *J. Non-Cryst. Solids* **1976**, *21*, 343–372. [[CrossRef](#)]
16. Kracek, F.C. The ternary system $K_2SiO_3-Na_2SiO_3-SiO_2$. *J. Phys. Chem.* **1932**, *36*, 2529–2542. [[CrossRef](#)]
17. Selvi, S.; Marimuthu, K.; Muralidharan, G. Structural and luminescence behavior of Sm^{3+} ions doped lead boro-telluro-phosphate glasses. *J. Lumin.* **2015**, *159*, 207–218. [[CrossRef](#)]
18. Muralidharan, M.N.; Rasmitha, C.A.; Rateesh, R. Photoluminescence and FTIR studies of pure and rare earth doped silica xerogels and aerogels. *J. Porous Mater.* **2009**, *16*, 635–640. [[CrossRef](#)]
19. Sanders, D.M.; Person, W.B.; Hench, L.L. Quantitative-analysis of glass structure with the use of infrared reflection spectra. *Appl. Spectrosc.* **1974**, *28*, 247–255. [[CrossRef](#)]
20. Matson, D.W.; Sharma, S.K.; Philpotts, J.A. The structure of high-silica alkali-silicate glasses—A Raman spectroscopy investigation. *J. Non-Cryst. Solids* **1983**, *58*, 323–352. [[CrossRef](#)]
21. El-Okr, M.; Ibrahim, M.; Farouk, M. Structure and properties of rare-earth-doped glassy systems. *J. Non-Cryst. Solids* **2008**, *69*, 2564–2567. [[CrossRef](#)]
22. Srinvasa Rao, C.; Srikumar, T.; Rao, M.C. Physical and optical absorption studies on LIF/NaF/KF- $P_2O_5-B_2O_3$ glasses doped with Sm_2O_3 . *IJCRGG* **2014**, *7*, 420–425.
23. Bhatia, B.; Meena, S.L.; Parihar, V.; Poonia, M. Optical basicity and polarizability of Nd^{3+} -doped bismuth borate glasses. *New J. Glass Ceram.* **2015**, *5*, 44–52. [[CrossRef](#)]
24. Judd, B.R. Optical absorption intensities of rare earth ions. *Phys. Rev.* **1962**, *127*, 750–761. [[CrossRef](#)]
25. Ofelt, G.S. Intensities of crystal spectra of rare earth ions. *J. Chem. Phys.* **1962**, *37*, 511–520. [[CrossRef](#)]

26. Jayasimhadri, M.; Moorthy, L.R.; Saleem, S.A.; Ravikumar, R.V.S.S. Spectroscopic characteristics of Sm³⁺-doped alkali fluorophosphate glasses. *Spectrochim. Acta Part A* **2006**, *64*, 939–944. [[CrossRef](#)]
27. Jayasankar, C.K.; Rukmini, E. Optical properties of Sm³⁺ ions in zinc and alkali zinc borosulphate glasses. *Opt. Mater.* **1997**, *8*, 193–205. [[CrossRef](#)]
28. Chen, B.J.; Shen, L.F.; Pun, E.Y.B.; Lin, H. Sm³⁺-doped germanate glass channel waveguide as light source for minimally invasive photodynamic therapy surgery. *Opt. Express* **2012**, *20*, 879–889. [[CrossRef](#)]
29. Jorgenson, C.K. *Orbitals Atoms and Molecules*; Academic Press: London, UK, 1962.
30. Sinha, S.P. *Complexes of the Rare Earth*; Pergamon Press: Oxford, UK, 1966.
31. Carnall, W.T.; Crosswhite, H.; Crosswhite, H.M. *Energy Level Structure and Transition Probabilities of the Trivalent Lanthanides in LaF₃*; Report ANL-78-XX-95; Argonne National Laboratory: Lemont, IL, USA, 1978.
32. Sudhakar, K.S.V.; Srinivasa Reddy, M.; Srinivasa Rao, L.; Veeraiah, N. Influence of modifier oxide on spectroscopic and thermoluminescence characteristics of Sm³⁺ ion in antimony borate glass system. *J. Lumin.* **2008**, *128*, 1791–1798. [[CrossRef](#)]
33. Rajesh, D.; Balakrishna, A.; Ratnakaram, Y.C. Luminescence, structural and dielectric properties of Sm³⁺ impurities in strontium lithium bismuth borate glasses. *Opt. Mater.* **2012**, *35*, 108–116. [[CrossRef](#)]
34. Ratnakaram, Y.C.; Thirupathi Naidu, D.; Chakradhar, R.P.S. Spectral studies of Sm³⁺ and Dy³⁺ doped lithium cesium mixed alkali borate glasses. *J. Non-Cryst. Solids* **2006**, *353*, 3914–3922. [[CrossRef](#)]
35. Takebe, H.; Nageno, Y.; Morinaga, K. Compositional dependence of Judd-Ofelt parameters in silicate, borate, and phosphate glasses. *J. Am. Ceram. Soc.* **1995**, *78*, 1161–1168. [[CrossRef](#)]
36. Shanmuga Sundari, S.; Marimuthu, K.; Sivraman, M.; Surendra Babu, S. Composition dependent structural and optical properties of Sm³⁺-doped sodium borate and sodium fluoroborate glasses. *J. Lumin.* **2010**, *130*, 1313–1319. [[CrossRef](#)]
37. Arul Rayappan, I.; Selvaraju, K.; Marimuthu, K. Structural and luminescence investigations on Sm³⁺ doped sodium fluoroborate glasses containing alkali/alkaline earth metal oxides. *Phys. B* **2011**, *406*, 548–555. [[CrossRef](#)]
38. Herrera, A.; Fernandes, R.G.; de Camargo, A.S.S.; Hernandez, A.C.; Buchner, S.; Jacinto, C.; Balzaretto, N.M. Visible–NIR emission and structural properties of Sm³⁺ doped heavy-metal oxide glass with composition B₂O₃–PbO–Bi₂O₃–GeO₂. *J. Lumin.* **2016**, *171*, 106–111. [[CrossRef](#)]
39. Montoya, I.M.; Balzaretto, N.M. High pressure effect on structural and spectroscopic properties of Sm³⁺ doped alkali silicate glasses. *High-Press. Res.* **2017**, *37*, 296–311. [[CrossRef](#)]

Disclaimer/Publisher’s Note: The statements, opinions and data contained in all publications are solely those of the individual author(s) and contributor(s) and not of MDPI and/or the editor(s). MDPI and/or the editor(s) disclaim responsibility for any injury to people or property resulting from any ideas, methods, instructions or products referred to in the content.